Hindawi
International Journal of Antennas and Propagation
Volume 2023, Article ID 1295821, 14 pages
https://doi.org/10.1155/2023/1295821

Research Article

Relativistic Bistatic Scattering of a High-Speed Moving Plasma Coated Object

Pengcheng Ren,[1,2] **Lei Kuang**,[1] **Jianjun Gao**,[2] **and Qing Huo Liu**[3]

[1]*Shanghai Key Laboratory of Multidimensional Information Processing, School of Communication and Electronic Engineering, East China Normal University, Shanghai 200241, China*
[2]*School of Physics and Electronic Science, East China Normal University, Shanghai 200241, China*
[3]*Department of Electrical and Computer Engineering, Duke University, Durham, NC 27708, USA*

Correspondence should be addressed to Lei Kuang; lkuang@ee.ecnu.edu.cn

Received 20 December 2022; Revised 12 April 2023; Accepted 13 April 2023; Published 25 April 2023

Academic Editor: Shah Nawaz Burokur

Accurate modeling of relativistic electromagnetic scattering characteristics from high-speed motion of plasma coated objects is crucial for the development of hypersonic aircraft and their applications in the identification and surveillance of moving stealth targets. Nevertheless, a solution for bistatic polarized radar cross sections (RCSs) from a 3-D object with plasma coated layer in motion has yet to be obtained. This manuscript proposes a solution to this problem by employing a combination of the auxiliary differential equation (ADE) method with Lorentz finite-difference time-domain (FDTD) method. Utilizing the Lorentz transformation, this paper presents the transformation of parameters of the incident plane wave and dimensions of the object between the laboratory system that remains static and the rest system that remains stationary relative to the object in high-speed motion. The near-zone electromagnetic fields near the object are computed using the ADE method in the rest system, after which the near-field to far-field (NF-FF) transformation is employed to obtain the far-zone polarized scattered field. By applying Lorentz transformation to the coordinates, this paper presents a solution for the polarized scattering from moving plasma coated objects. Especially, radial components of the polarized scatterings are analyzed. The proposed method is validated through several numerical experiments, demonstrating its efficiency and accuracy.

1. Introduction

In recent years, there has been significant interest in the analysis of electromagnetic scattering from high-speed moving objects, driven by the rapid progress of high-speed target. In particular, there is a growing focus on investigating EM scattering characteristics of moving plasma coated targets due to their superior stealth performance. Such investigations have practical applications in the detection and analysis of high-speed stealth moving objects. The plasma layer is typically considered as an isotropic and dispersive medium, satisfying the single-pole Drude model. To simulate such materials, the FDTD algorithm [1] has become a popular choice due to its simplicity relative to analytic methods and other numerical algorithms. Basically, the available frequency dispersive FDTD algorithms can be divided into three categories, and all of these are based on the polarization equation which constructs the relationship between the electric flux density and the electric field intensity. In the first type which is called recursive convolution (RC) approach [2, 3], the electric flux density is proposed to be combined with the electric field density through a convolution integral. Based on this theory, several modified RC schemes such as the piecewise linear recursive convolution (PLRC) [4] and the trapezoidal rule recursive convolution (TRC) [5] are presented to obtain the second-order accuracy in time while modeling the dispersive media. The dispersive FDTD algorithm based on the RC scheme has been applied for modeling of different types of dispersive materials in [6–8]. However, the formulation of the RC scheme is

complex, and the implementation of the derivation process is also difficult. The second approach involves reducing the convolution integral in the time domain to a multiplication through the implementation of Z-transform, and a recursive relationship between electric flux density and electric field can be obtained [9]. However, the transformation between the time domain and Z domain requires complex arithmetic which lowers the computational efficiency of this scheme. In the third approach, the polarization vector and the electric flux density are linked utilizing ADE method [10–12]. Thus, Maxwell's curl equations and the ADE method from a system are solved recursively by the FDTD algorithm. Due to the implementation of the ADE method to describe the frequency-dependent material properties [12–17], it is worth noting that among the various numerical methods, the ADE method can achieve an optimal balance between computational efficiency and accuracy compared to the other frequency dispersive FDTD algorithms. However, the algorithms discussed above concentrate exclusively on electromagnetic analysis of dispersive media that are stationary.

The motion of an object at high speeds leads to modulation of the scattering wave's frequency and amplitude, and it is crucial to consider this phenomenon in any accurate solution to the object's scattering property. Einstein's special relativity theory provides the necessary foundation for developing such a solution. As a result, more attention is being paid to the development of efficient models that can effectively simulate moving objects. So far, researchers have made significant contributions to the development of various theoretical and numerical solutions for relativistic electromagnetic scattering of moving objects. The frame hopping method (FHM) is an analytical method based on the theory of relativity, which solves the scattering fields in the comoving frame and transforms the scattering fields back to the laboratory frame. The FHM method is used to obtain the exact solution of the scattering from a perfectly conducting half plane in relativistic uniform motion in [18]. Despite significant progress in analytical and asymptotic methods, obtaining exact scattering solutions for arbitrarily shaped and composed moving objects remains a challenging task.

In recent years, the FDTD algorithm has emerged as a popular tool for analyzing the scattering from moving objects. Two primary categories of algorithms have been developed to solve for relativistic scatterings of moving objects. The first algorithm involves direct solutions that employ the relativistic boundary condition (RBC) [19–21] to the boundary surface in motion between two media in the FDTD simulation, known as the RBC-FDTD algorithm. Nevertheless, this algorithm can be susceptible to numerical instability issues arising from the discrete interpolation of the electromagnetic field on the boundary surface in motion at each time step. An alternative method for modeling the electromagnetic scattering from objects in high-speed motion is the Lorentz-FDTD method that involves converting parameters of the incident plane wave to the rest system relative to the moving object through the implementation of Lorentz transformation. The far-zone scattered fields of the moving object are then solved using the FDTD algorithm in the rest system and subsequently converted back into the laboratory system, completing the Lorentz-FDTD method. This method is considered a viable alternative to the RBC-FDTD algorithm and has gained attention in recent years due to its accuracy and stability. During the recent years, the Lorentz-FDTD method has become increasingly recognized for its effectiveness in solving relativistic scattering problems. This method circumvents the need for field interpolation on the moving interface and is considered more numerically stable than the RBC-FDTD method. As a result, the Lorentz-FDTD method has become the preferred approach for addressing relativistic scattering problems. The Lorentz-FDTD method has been employed to investigate double Doppler effects of scatterings from moving conducting surfaces [22] and moving dielectric slabs [23] at various velocities when the incident plane wave is introduced into the rest system. This analysis provided insight into the scattering from high-speed moving objects and demonstrated the effectiveness of the Lorentz-FDTD method in accurately modeling such phenomena. The Lorentz-FDTD method was employed to analyze the bistatic radar cross sections of 2-D objects in uniform motion, which consisted of both conducting and dielectric materials. Through this analysis, the Doppler effect was studied, considering quantities of the incident plane wave and scattered wave. The results of this analysis were presented in [24], providing valuable insights into the scattering properties of moving objects and further demonstrating the efficacy of the Lorentz-FDTD method in solving complex electromagnetic scattering problems. To investigate the scattering properties of a 3-D irregularly-shaped object in motion, the Lorentz-FDTD method is employed to solve scattering problems. This analysis was presented in [25], and the successful implementation of the Lorentz-FDTD method demonstrates its potential for solving scattering problems involving 3-D complex moving structures. The transmitted and reflected waves by a 2-D left-handed metamaterial (LHM) slab in high-speed motion are investigated using a combination of the Lorentz-FDTD method and the ADE method, as presented in [26]. Due to the study target is a 2-D LHM slab in high-speed motion, it is not possible to obtain the polarized RCS. By employing the boundary perturbation method in conjunction with the Lorentz transformation, scatterings of electromagnetic wave from rough surfaces in motion were investigated in the study presented in [27]. In addition, the study presents the radial scattering cross sections that are exclusively attributed to the motion of the scatter. Despite the advancements made in the asymptotic method described in [27], exact solutions for the scattering of objects in high-speed motion with arbitrary shapes and compositions still pose a significant challenge. In [28], the Lorentz-FDTD method is employed to solve the problem of relativistic polarized RCSs of a dielectric-coated target in high-speed motion. So far, there has been no investigation into the far-zone polarized scatterings from 3-D objects in high-speed motion with the plasma coating layer.

In this research, we proposed the Lorentz-ADE-FDTD algorithm combining the ADE method with Lorentz-FDTD method to solve for the relativistic far-zone polarized scatterings of a 3-D plasma coated object

in high-speed motion. The manuscript is structured as follows: In Section 2, the quantities of incident plane wave between the rest system Ω' with the respect to the moving object and the laboratory system Ω relative to the free space are presented. A concise overview of the ADE method is provided, and we outline its implementation for computing the near-field data of the 3-D plasma object in high-speed motion which satisfies the Drude model in the rest system. Sections 3, respectively, presents the computation of the far-zone scattered field and the RCS of the moving target using the proposed Lorentz-ADE-FDTD algorithm. Section 4 discusses the simulated results that demonstrate the efficiency and accuracy of the Lorentz-ADE-FDTD algorithm. In Section 5, the findings of this study are concluded and discussed.

2. Lorentz-ADE-FDTD Formulation

The previous works [25] have detailed described the transformation formulas of the incident plane wave using the Lorentz-FDTD method. Assume that an object is in motion along x axis at a velocity of v. Therefore, correspondence relationships between unprimed quantities of the incident plane wave in the laboratory system Ω, which is stationary with respect to the free space and primed quantities of the incident plane wave in the rest system Ω' relative to the object in motion, can be presented as

$$E_0' = E_0\gamma\left(1 - \beta\sin\theta_i\cos\varphi_i\right), \tag{1a}$$

$$k_i' = k_i\gamma\left(1 - \beta\sin\theta_i\cos\varphi_i\right), \tag{1b}$$

$$\omega_i' = \omega_i\gamma\left(1 - \beta\sin\theta_i\cos\varphi_i\right), \tag{1c}$$

$$\sin\theta_i' = \frac{\sqrt{\gamma^2\left(\sin\theta_i\cos\varphi_i - \beta\right)^2 + \sin^2\theta_i\sin^2\varphi_i}}{\gamma\left(1 - \beta\sin\theta_i\cos\varphi_i\right)}, \tag{1d}$$

$$\cos\theta_i' = \frac{\cos\theta_i}{\gamma\left(1 - \beta\sin\theta_i\cos\varphi_i\right)}, \tag{1e}$$

$$\sin\varphi_i' = \frac{\sin\theta_i\sin\varphi_i}{\sqrt{\gamma^2\left(\sin\theta_i\cos\varphi_i - \beta\right)^2 + \sin^2\theta_i\sin^2\varphi_i}}, \tag{1f}$$

$$\cos\varphi_i' = \frac{\gamma\left(\sin\theta_i\cos\varphi_i - \beta\right)}{\sqrt{\gamma^2\left(\sin\theta_i\cos\varphi_i - \beta\right)^2 + \sin^2\theta_i\sin^2\varphi_i}}, \tag{1g}$$

$$\sin\alpha' = \frac{\gamma\left(\sin\theta_i\sin\alpha - \beta\cos\varphi_i\sin\alpha - \beta\sin\varphi_i\cos\theta_i\cos\alpha\right)}{\sqrt{\gamma^2\left(\sin\theta_i\cos\varphi_i - \beta\right)^2 + \sin^2\theta_i\sin^2\varphi_i}}, \tag{1h}$$

$$\cos\alpha' = \frac{\gamma\left(\sin\theta_i\cos\alpha - \beta\cos\varphi_i\cos\alpha + \beta\sin\varphi_i\cos\theta_i\sin\alpha\right)}{\sqrt{\gamma^2\left(\sin\theta_i\cos\varphi_i - \beta\right)^2 + \sin^2\theta_i\sin^2\varphi_i}}. \tag{1i}$$

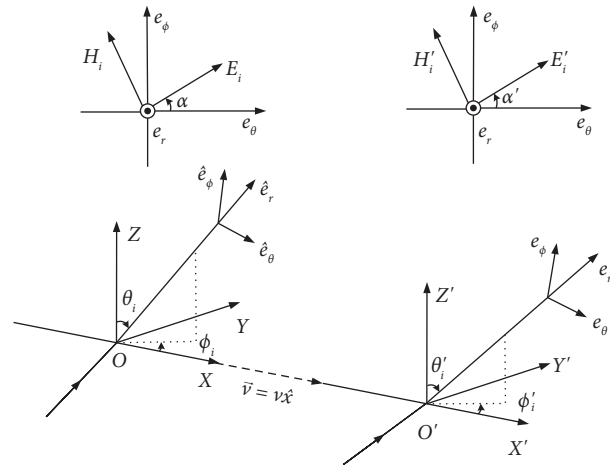

Figure 1: Transformation between incident plane waves in the laboratory system and in the rest system.

As illustrated in Figure 1, θ_i, φ_i are the incident angles, α represents the polarizing angle of the incident plane wave, k_i denotes the wavenumber of the incident plane wave, ω_i is the angular velocity of the incident plane wave, Z_0 denotes the intrinsic impendence, and E_0 represents the electric field amplitude of the incident plane wave. The definition of the quantities β and γ is expressed as follows:

$$\beta = v/c, \tag{2a}$$

$$\gamma = 1/\sqrt{1 - \beta^2}, \tag{2b}$$

where c denotes the velocity of light in vacuum.

According to transformation relations of quantities of the incident plane wave between system Ω and system Ω', the incident plane wave can be converted from system Ω to system Ω' in order to excite the object. The computation domain is meshed by applying the Yee grid algorithm, and the boundary of the computation domain is truncated by the implementation of convolutional perfectly matched layer (CPML) to absorb outward-propagating waves. The total-field scattered-field (TF-SF) connecting boundary technology is then applied to introduce the transformed incident plane wave into the total-field domain. By applying the ADE iteration equations, scattered near field of the plasma coated object in system Ω' can be obtained.

Maxwell's curl equation converted into discretized time domain equation applying the central-difference approximation can be written as

$$\left[\nabla \times \vec{H}^{n+1/2}\right] = \varepsilon_0\varepsilon_\infty\frac{\vec{E}^{n+1} - \vec{E}^{n}}{\Delta t'} + \sigma\frac{\vec{E}^{n+1} + \vec{E}^{n}}{2} + \frac{\vec{J}_p^{n+1} + \vec{J}_p^{n}}{2}, \tag{3}$$

where $\Delta t'$ represents the time incremental step in system Ω'. The expression of $\Delta t'$ is given by

$$\Delta t^{'} = \frac{1}{c\sqrt{1/\left(\Delta x^{'}\right)^{2} + 1/\left(\Delta y^{'}\right)^{2} + 1/\left(\Delta z^{'}\right)^{2}}}, \tag{4}$$

where $\Delta x^{'}$, $\Delta y^{'}$, and $\Delta z^{'}$ represent the spatial incremental step in system $\Omega^{'}$. The transformation relationships between the spatial incremental steps between system $\Omega^{'}$ and system Ω are expressed as

$$\Delta x^{'} = \gamma \Delta x, \tag{5a}$$

$$\Delta y^{'} = \Delta y, \tag{5b}$$

$$\Delta z^{'} = \Delta z. \tag{5c}$$

The phasor polarization current $\vec{J}_p$ in the frequency domain is presented as

$$\vec{J}_p(\omega) = j\omega\varepsilon_0\chi(\omega)\vec{E}(\omega), \tag{6}$$

where j represents the imaginary unit. The plasma involved in this paper can be regraded as isotropic and frequency-dependent material. The permittivity of the plasma can be described by the single-pole Drude model and presented as

$$\chi(\omega) = \frac{-\omega_p^2}{\omega\left(\omega - j\nu_c\right)}, \tag{7}$$

where ω_p denotes the frequency of the Drude model; ν_c is the collision frequency.

Substitute the equation (7) into the equation (6), the phasor polarization current $\vec{J}_p$ in the frequency domain can be rewritten as

$$\vec{J}_p(\omega) = j\omega\varepsilon_0\chi(\omega)\vec{E}(\omega) = -j\omega\varepsilon_0\frac{\omega_p^2}{\omega\left(\omega - j\nu_c\right)}\vec{E}(\omega). \tag{8}$$

Transform the above equation into time domain, we can get

$$\frac{\partial \vec{J}_p}{\partial t} + \nu_c\vec{J}_p = \varepsilon_0\omega_p^2\vec{E}. \tag{9}$$

Applying the central-difference approximation to discrete the equation (8), we can yield

$$\vec{J}_p^{\,n+1} = k_p\vec{J}_p^{\,n} + \beta_p\left(\vec{E}^{\,n+1} + \vec{E}^{\,n}\right), \tag{10}$$

$$k_p = \frac{2 - \nu_c\Delta t^{'}}{2 + \nu_c\Delta t^{'}}, \tag{11a}$$

$$\beta_p = \frac{\omega_p^2\varepsilon_0\Delta t^{'}}{2 + \nu_c\Delta t^{'}}. \tag{11b}$$

Substitute the equation (10) into the equation (3), the updated equation of the E components in system $\Omega^{'}$ is written as

$$\vec{E}_x^{\,n+1} = CA\cdot\vec{E}_x^{\,n} + CB\cdot\left\{\left[\nabla\times\vec{H}^{\,n+1/2}\right]_x - \frac{1}{2}\left(1 + k_p\right)\vec{J}_p^{\,n}\right\}, \tag{12a}$$

$$\vec{E}_y^{\,n+1} = CA\cdot\vec{E}_y^{\,n} + CB\cdot\left\{\left[\nabla\times\vec{H}^{\,n+1/2}\right]_y - \frac{1}{2}\left(1 + k_p\right)\vec{J}_p^{\,n}\right\}, \tag{12b}$$

$$\vec{E}_z^{\,n+1} = CA\cdot\vec{E}_z^{\,n} + CB\cdot\left\{\left[\nabla\times\vec{H}^{\,n+1/2}\right]_z - \frac{1}{2}\left(1 + k_p\right)\vec{J}_p^{\,n}\right\}, \tag{12c}$$

where

$$CA = \frac{2\varepsilon_0\varepsilon_\infty - \beta_p\Delta t^{'} - \sigma\Delta t^{'}}{2\varepsilon_0\varepsilon_\infty + \beta_p\Delta t^{'} + \sigma\Delta t^{'}}, \tag{13a}$$

$$CB = \frac{2\Delta t^{'}}{2\varepsilon_0\varepsilon_\infty + \beta_p\Delta t^{'} + \sigma\Delta t^{'}}. \tag{13b}$$

It should be noted that the E field components which are not involved in the plasma layer should be computed using the conventional FDTD method.

3. Polarized Scattering of the Moving Object

After obtaining the near-field data in the scattered field domain, we employ NF-FF transformation to obtain the electromagnetic scattered far-field of the object in system $\Omega^{'}$. According to the derivation of the electromagnetic scattered far-field described in reference [1], the scattered far-fields are given by with respect to the Cartesian coordinate system as follows:

$$E_{sx}^{'} = \mathrm{j}k_s' \left\{ \begin{array}{l} -F_y \cos\theta_s' + F_z \sin\theta_s' \sin\varphi_s' - Z_0 A_x \left(1 - \sin^2\theta_s' \cos^2\varphi_s'\right) \\ +Z_0 A_y \sin^2\theta_s' \sin\varphi_s' \cos\varphi_s' + Z_0 A_z \sin\theta_s' \cos\theta_s' \cos\varphi_s' \end{array} \right\}, \tag{14a}$$

$$E_{sy}^{'} = \mathrm{j}k_s' \left\{ \begin{array}{l} -F_z \sin\theta_s' \cos\varphi_s' + F_x \cos\theta_s' - Z_0 A_y \left(1 - \sin^2\theta_s' \sin^2\varphi_s'\right) \\ +Z_0 A_x \sin^2\theta_s' \sin\varphi_s' \cos\varphi_s' + Z_0 A_z \sin\theta_s' \cos\theta_s' \sin\varphi_s' \end{array} \right\}, \tag{14b}$$

$$E_{sz}^{'} = \mathrm{j}k_s' \left\{ \begin{array}{l} F_y \sin\theta_s' \cos\varphi_s' - F_x \sin\theta_s' \sin\varphi_s' - Z_0 A_z \left(1 - \cos^2\theta_s'\right) \\ +Z_0 A_x \sin\theta_s' \cos\theta_s' \cos\varphi_s' + Z_0 A_y \sin\theta_s' \cos\theta_s' \sin\varphi_s' \end{array} \right\}, \tag{14c}$$

$$H_{sx}^{'} = \mathrm{j}k_s' \left\{ \begin{array}{l} A_y \cos\theta_s' - A_z \sin\theta_s' \sin\varphi_s' - \dfrac{F_x}{Z_0} \left(1 - \sin^2\theta_s' \cos^2\varphi_s'\right) \\ +\dfrac{F_y}{Z_0} \sin^2\theta_s' \sin\varphi_s' \cos\varphi_s' + \dfrac{F_z}{Z_0} \sin\theta_s' \cos\theta_s' \cos\varphi_s' \end{array} \right\}, \tag{14d}$$

$$H_{sy}^{'} = \mathrm{j}k_s' \left\{ \begin{array}{l} A_z \sin\theta_s' \cos\varphi_s' - A_x \cos\theta_s' - \dfrac{F_y}{Z_0} \left(1 - \sin^2\theta_s' \sin^2\varphi_s'\right) \\ +\dfrac{F_x}{Z_0} \sin^2\theta_s' \sin\varphi_s' \cos\varphi_s' + \dfrac{F_z}{Z_0} \sin\theta_s' \cos\theta_s' \sin\varphi_s' \end{array} \right\}, \tag{14e}$$

$$H_{sz}^{'} = \mathrm{j}k_s' \left\{ \begin{array}{l} A_x \sin\theta_s' \sin\varphi_s' - A_y \sin\theta_s' \cos\varphi_s' - \dfrac{F_z}{Z_0} \left(1 - \cos^2\theta_s'\right) \\ +\dfrac{F_x}{Z_0} \sin\theta_s' \cos\theta_s' \cos\varphi_s' + \dfrac{F_y}{Z_0} \sin\theta_s' \cos\theta_s' \sin\varphi_s' \end{array} \right\}, \tag{14f}$$

where

$$A_\zeta = \frac{\exp\left(-\mathrm{j}k_s' R^{'}\right)}{4\pi R^{'}} \int_{S_v} J_\zeta^{'e} \exp\left(\mathrm{j}k_s' x^{'} \sin\theta_s' \cos\varphi_s' + \mathrm{j}k_s' y^{'} \sin\theta_s' \sin\varphi_s' + \mathrm{j}k_s' z^{'} \cos\theta_s'\right) \mathrm{d}s, \tag{15a}$$

$$F_\zeta = \frac{\exp\left(-\mathrm{j}k_s' R^{'}\right)}{4\pi R^{'}} \int_{S_v} J_\zeta^{'m} \exp\left(\mathrm{j}k_s' x^{'} \sin\theta_s' \cos\varphi_s' + \mathrm{j}k_s' y^{'} \sin\theta_s' \sin\varphi_s' + \mathrm{j}k_s' z^{'} \cos\theta_s'\right) \mathrm{d}s, \tag{15b}$$

where ζ is selected as x, y and z, respectively; $\vec{J}^{'e}$ and $\vec{J}^{'m}$ are equivalent surface electric current and equivalent surface magnetic currents on the imaginary surface selected to enclose the object in the scattered field domain, respectively; k_s' denotes the wavenumber of the scattered wave in system $\Omega^{'}$, which is equivalent to k_i'.

The Lorentz transformation formulations can be employed to transform the scattered electromagnetic far-fields in system $\Omega^{'}$ back to system Ω using the following equations:

$$E_{sx} = E_{sx}^{'}, \tag{16a}$$

$$E_{sy} = \gamma\left(E_{sy}^{'} + v \cdot \mu \cdot H_{sz}^{'}\right), \tag{16b}$$

$$E_{sz} = \gamma\left(E_{sz}^{'} - v \cdot \mu \cdot H_{sy}^{'}\right). \tag{16c}$$

The electromagnetic scattering problem typically involves the consideration of polarized scattered field components, which are oriented parallel and perpendicular to

the plane of scattering. However, in doing so, the expression for the scatterings of the moving object becomes intractable. According to [27], the transformation of the three polarized scattered electric fields between the rectangular coordinate system (O, X, Y, Z) and the Galilean spherical coordinate system $(O_G, r(t), \theta_s(t), \varphi_s(t))$ can be expressed as follows:

$$\begin{pmatrix} E_{sh} \\ E_{sv} \\ E_{sr} \end{pmatrix} = \begin{pmatrix} -\sin\varphi_s(t) & \cos\varphi_s(t) & 0 \\ \cos\theta_s(t)\cos\varphi_s(t) & \cos\theta_s(t)\sin\varphi_s(t) & -\sin\theta_s(t) \\ \sin\theta_s(t)\cos\varphi_s(t) & \sin\theta_s(t)\sin\varphi_s(t) & \cos\theta_s(t) \end{pmatrix} \begin{pmatrix} E_{sx} \\ E_{sy} \\ E_{sz} \end{pmatrix}, \tag{17}$$

where E_{sx}, E_{sy}, and E_{sz} are derived from equations (16a)–(16c).

As shown in Figure 2, R is applied to represents the distance between the observation point $P(x_0, y_0, z_0)$ and the origin point O.

The bistatic polarized RCS of the 3-D object in motion, which denotes the electromagnetic power scattered towards $P(x_0, y_0, z_0)$, can be expressed as follows:

$$\sigma_{qp}(\theta_i, \varphi_i, \theta_s, \varphi_s) = \lim_{R\longrightarrow\infty} 10\lg\left(4\pi R^2\left|\frac{E_q}{E_p}\right|^2\right)(\text{dB sm}), \tag{18}$$

where $q = v, h, r$ denotes scattered electric fields with three types of polarization, respectively; $p = h, v$ denotes the incident electric fields with two types of polarization, respectively. The definitions of v, h, and r are presented: v represents the vertical polarized component; h represents the horizontal polarized component; r represents the radial scattering component. The formulas of the scattered electric fields contain quantities of the scattering wave involved in system Ω'. The crucial process in computing the solutions of different polarized scattering of an object in high-speed motion is to establish relationships of the quantities of the scattering wave between the two systems, which can be obtained by the combination between Lorentz transformation and the geometrical relationship.

As depicted in Figure 2, as the observation distance R approaches infinity, we can observe that

$$\lim_{R\longrightarrow\infty} r(t) = R, \tag{19a}$$

$$\lim_{R\longrightarrow\infty} \theta_s(t) = \theta_s, \tag{19b}$$

$$\lim_{R\longrightarrow\infty} \varphi_s(t) = \varphi_s. \tag{19c}$$

Based on the geometrical relationship between the triangle $P'O'P''$ and the triangle $P'O_GP''$, it is possible to prove that

$$\lim_{R\longrightarrow\infty} \sin\varphi_s' = \sin\varphi_s \frac{\sqrt{1-\beta^2}}{\sqrt{1-\beta^2\sin^2\varphi_s}}, \tag{20a}$$

$$\lim_{R\longrightarrow\infty} \cos\varphi_s' = \cos\varphi_s \frac{1}{\sqrt{1-\beta^2\sin^2\varphi_s}}. \tag{20b}$$

Based on the geometrical relationship, transformation relationships between quantities of the scattering wave in system Ω and corresponding quantities in system Ω' are shown as follows:

$$\lim_{R\longrightarrow\infty} \cos\theta_s' = \cos\theta_s \frac{\sqrt{1-\beta^2}}{\sqrt{1-\beta^2\left(\cos^2\theta_s + \sin^2\theta_s\sin^2\varphi_s\right)}}, \tag{20c}$$

$$\lim_{R\longrightarrow\infty} \sin\theta_s' = \sin\theta_s \frac{\sqrt{1-\beta^2\sin^2\varphi_s}}{\sqrt{1-\beta^2\left(\cos^2\theta_s + \sin^2\theta_s\sin^2\varphi_s\right)}}, \tag{20d}$$

$$\lim_{R\longrightarrow\infty} \frac{R}{R'} = \frac{\sqrt{1-\beta^2}}{\sqrt{1-\beta^2\left(\cos^2\theta_s + \sin^2\theta_s\sin^2\varphi_s\right)}}. \tag{20e}$$

Combination of (20a)–(20e), (14a)–(14f), (15a) and (15b), (16a)–(16c), (17), and (18) leads to the acquirement for the bistatic polarized RCS from the moving object. It is worth noting that the movement of the object introduces a new component E_{sr}, which remains absent in the case of a stationary object.

For the static case of the object, the expressions of the components β, γ are modified as follows:

$$\beta = \frac{v}{c} = 0, \tag{21a}$$

$$\gamma = \frac{1}{\sqrt{1-\beta^2}} = 1. \tag{21b}$$

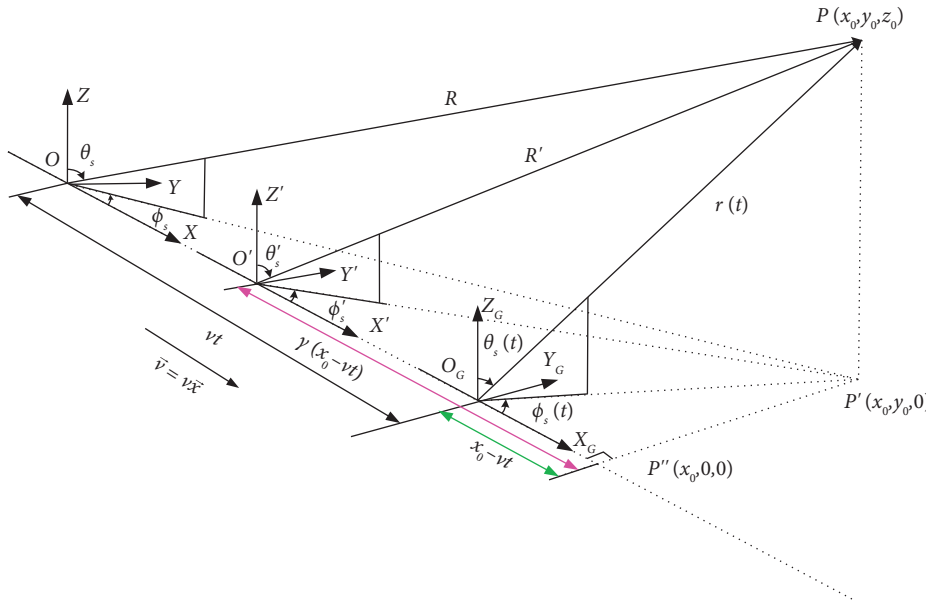

Figure 2: Scattering geometry.

Substitute formulation (21a) and (21b) into formulation (20a)–(20e), the relationships between quantities in system Ω' and corresponding quantities in system Ω are rewritten as follows:

$$\sin\varphi_s' = \sin\varphi_s, \tag{22a}$$

$$\cos\varphi_s' = \cos\varphi_s, \tag{22b}$$

$$\cos\theta_s' = \cos\theta_s, \tag{22c}$$

$$\sin\theta_s' = \sin\theta_s, \tag{22d}$$

$$R' = R. \tag{22e}$$

Meanwhile, substitute formulation (21a) and (21b) into (16a)–(16c), the modifications of the transformation between the scattered polarized far-fields in system Ω' and corresponding scattered electric fields in system Ω are presented as follows:

$$E_{sx} = E_{sx}', \tag{23a}$$

$$E_{sy} = E_{sy}', \tag{23b}$$

$$E_{sz} = E_{sz}'. \tag{23c}$$

Combination of formulation (22a)–(22e), (23a)–(23c), and (14a)–(14c) leads to the scattered electric field components corresponding to the Cartesian coordinate system which can be written as follows:

$$E_{sx} = jk_s'\left\{\begin{array}{l} -F_y\cos\theta_s + F_z\sin\theta_s\sin\varphi_s - Z_0A_x\left(1-\sin^2\theta_s\cos^2\varphi_s\right) \\ +Z_0A_y\sin^2\theta_s\sin\varphi_s\cos\varphi_s + Z_0A_z\sin\theta_s\cos\theta_s\cos\varphi_s \end{array}\right\}, \tag{24a}$$

$$E_{sy} = jk_s'\left\{\begin{array}{l} -F_z\sin\theta_s\cos\varphi_s + F_x\cos\theta_s + Z_0A_y\left(\sin^2\theta_s\sin^2\varphi_s - 1\right) \\ +Z_0A_x\sin^2\theta_s\sin\varphi_s\cos\varphi_s + Z_0A_z\sin\theta_s\cos\theta_s\sin\varphi_s \end{array}\right\}, \tag{24b}$$

$$E_{sz} = jk_s'\left\{\begin{array}{l} F_y\sin\theta_s\cos\varphi_s - F_x\sin\theta_s\sin\varphi_s + Z_0A_z\left(\cos^2\theta_s - 1\right) \\ +Z_0A_x\sin\theta_s\cos\theta_s\cos\varphi_s + Z_0A_y\sin\theta_s\cos\theta_s\sin\varphi_s \end{array}\right\}. \tag{24c}$$

Substitute the formulation (24a)–(24c) and (19a)–(19c) into formulation (17), the radial component of the scattered electric field from the static object can be expressed as follows:

$$
\begin{aligned}
E_{sr} = {} & jk_s' \sin\theta_s \cos\varphi_s \left\{ \begin{array}{l} F_z \sin\theta_s \sin\varphi_s - F_y \cos\theta_s + Z_0\left(\sin^2\theta_s \cos^2\varphi_s - 1\right)A_x \\ +Z_0 \sin^2\theta_s \sin\varphi_s \cos\varphi_s A_y + Z_0 \sin\theta_s \cos\theta_s \cos\varphi_s A_z \end{array} \right\} \\
& + jk_s' \sin\theta_s \sin\varphi_s \left\{ \begin{array}{l} F_x \cos\theta_s - F_z \sin\theta_s \cos\varphi_s + Z_0 \sin^2\theta_s \sin\varphi_s \cos\varphi_s A_x \\ +Z_0\left(\sin^2\theta_s \sin^2\varphi_s - 1\right)A_y + Z_0 \sin\theta_s \cos\theta_s \sin\varphi_s A_z \end{array} \right\} \\
& + jk_s' \cos\theta_s \left\{ \begin{array}{l} F_y \sin\theta_s \cos\varphi_s - F_x \sin\theta_s \sin\varphi_s + Z_0\left(\cos^2\theta_s - 1\right)A_z \\ +Z_0 \sin\theta_s \cos\theta_s \sin\varphi_s A_y + Z_0 \sin\theta_s \cos\theta_s \cos\varphi_s A_x \end{array} \right\}.
\end{aligned} \tag{25}
$$

After refreshing the above expression, we can get

$$
\begin{aligned}
E_{sr} = {} & jk_s' \left\{ \begin{array}{l} F_z\left(\sin^2\theta_s \sin\varphi_s \cos\varphi_s - \sin^2\theta_s \sin\varphi_s \cos\varphi_s\right) \\ +F_y\left(-\sin\theta_s \cos\theta_s \cos\varphi_s + \sin\theta_s \cos\theta_s \cos\varphi_s\right) \\ +F_x\left(\sin\theta_s \cos\theta_s \sin\varphi_s - \sin\theta_s \cos\theta_s \sin\varphi_s\right) \end{array} \right\} \\
& + jk_s' Z_0 A_x \begin{pmatrix} \sin^3\theta_s \cos^3\varphi_s + \sin\theta_s \cos^2\theta_s \cos\varphi_s \\ -\sin\theta_s \cos\varphi_s + \sin^3\theta_s \sin^2\varphi_s \cos\varphi_s \end{pmatrix} \\
& + jk_s' Z_0 A_y \begin{pmatrix} \sin^3\theta_s \sin^3\varphi_s + \sin\theta_s \cos^2\theta_s \sin\varphi_s \\ -\sin\theta_s \sin\varphi_s + \sin^3\theta_s \sin\varphi_s \cos^2\varphi_s \end{pmatrix} \\
& + jk_s' Z_0 A_z \begin{pmatrix} \cos^3\theta_s + \sin^2\theta_s \cos\theta_s \sin^2\varphi_s \\ -\cos\theta_s + \sin^2\theta_s \cos\theta_s \cos^2\varphi_s \end{pmatrix} \\
= {} & 0.
\end{aligned} \tag{26}
$$

It can be seen from the formulation (26) that the value of the radial scattering component for the static object is zero.

4. Numerical Results

In order to validate the Lorentz-ADE-FDTD algorithm, this section presents the results of several numerical cases. To verify the accuracy of the Lorentz-ADE-FDTD algorithm, the first case investigates the reflection coefficient of a slab in motion filled with plasma. To further verify the effectiveness of the Lorentz-ADE-FDTD algorithm, the second case analyzes the polarized scatterings from moving plasma objects. The other numerical cases are proposed to investigate the polarized RCSs from moving plasma coated objects. And the plasma used in the numerical cases can be regarded as the isotropic and dispersive medium, which satisfies the single-pole Drude model. It should be noted that the "FDTD-LT" in the following figures denotes the results obtained using the Lorentz-ADE-FDTD algorithm.

We have conducted an extra comparison of our method with respect to the previous analytical results in order to validate the Lorentz-ADE-FDTD algorithm. We compared the reflection coefficients of a moving plasma slab calculated by the Lorentz-ADE-FDTD algorithm with respect to the theoretical method presented in [29]. A 1-D moving plasma slab of thickness $d = 0.005$ m is considered in this case. The plasma frequency is $\omega_p = 6.8829 \times 10^{10}$rad/s. A harmonic incident plane wave is propagated towards the interface of the plasma slab in motion with its magnetic field linearly polarized along the y axis. The frequency is set to be 10 GHz.

The reflection coefficients are solved for incident angles ranging from 0° to 90°. Figure 3 presents reflection coefficients of the plasma slab in motion along x axis for velocities of $v = 0.1c$ and $v = 0$, respectively. The analytical results are calculated by applying formulations given by the authors of [29]. By comparison, Figure 3 shows a perfect agreement, which demonstrates the validity of the Lorentz-ADE-FDTD algorithm.

In this case, a plasma cylinder having the dimension of $r = 0.1$ m, $h = 0.4$ m is simulated to verify the accuracy of the Lorentz-ADE-FDTD algorithm. A sinusoidal plane wave with the frequency of 8 GHz is introduced into the computation domain via the connecting boundary technique formulation. We set the incident plane wave propagating along the y-direction with the electric field polarized along the z-direction. The plasma frequency ω_p is equal to 3.9845×10^{10}rad/s. The electron collision ν_c is $2\pi \times 10^{10}$rad/s.

The polarized (VH, HH, RH) bistatic RCS for the cases of velocity $v = 0$, $0.00001c$ (about Mach 8.82), $0.01c$, and $0.1c$m/s in the x-direction is shown in Figures 4(a)–4(c), respectively. The scattering angle θ_s is in the range from 0° to 360°. The scattering angle φ_s is 0°. The obtained results are further validated by comparing them with the theoretical

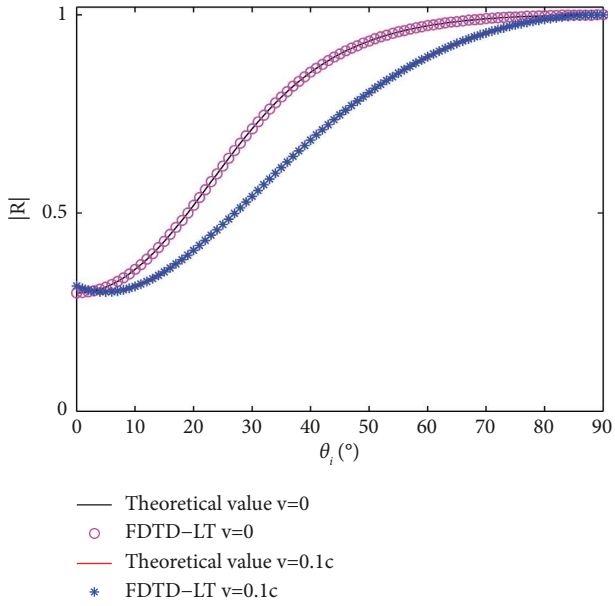

Figure 3: Reflection coefficients of the moving plasma slab.

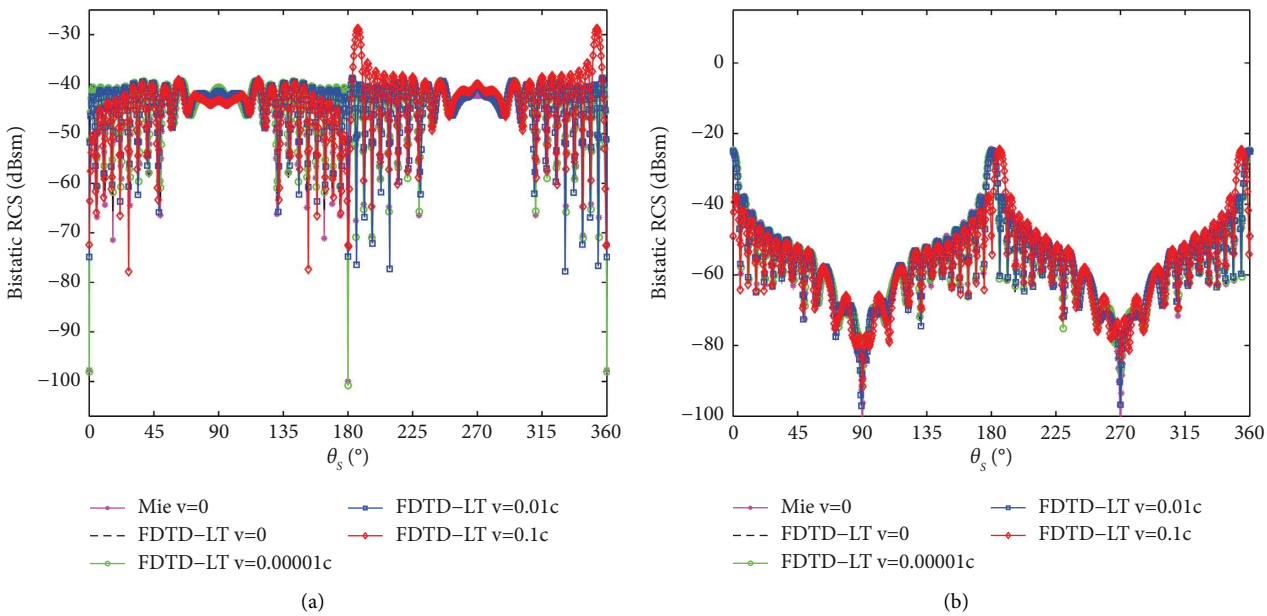

Figure 4: Continued.

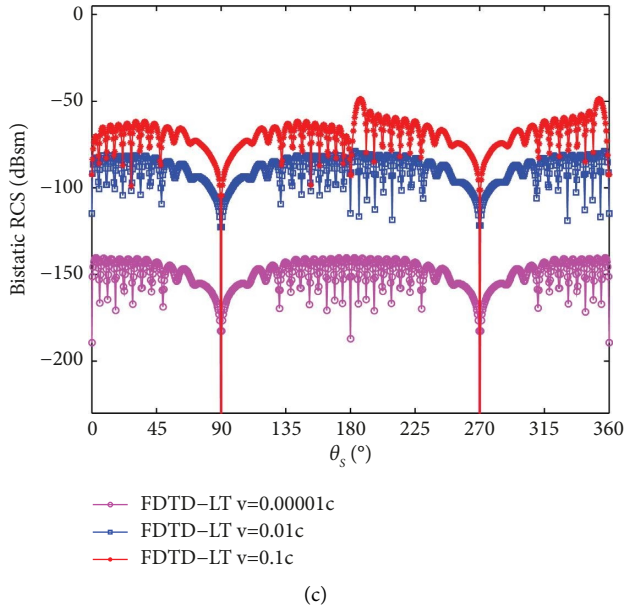

(c)

Figure 4: Polarized RCS for the plasma cylinder: (a) VH-polarization, (b) HH-polarization, and (c) RH-polarization.

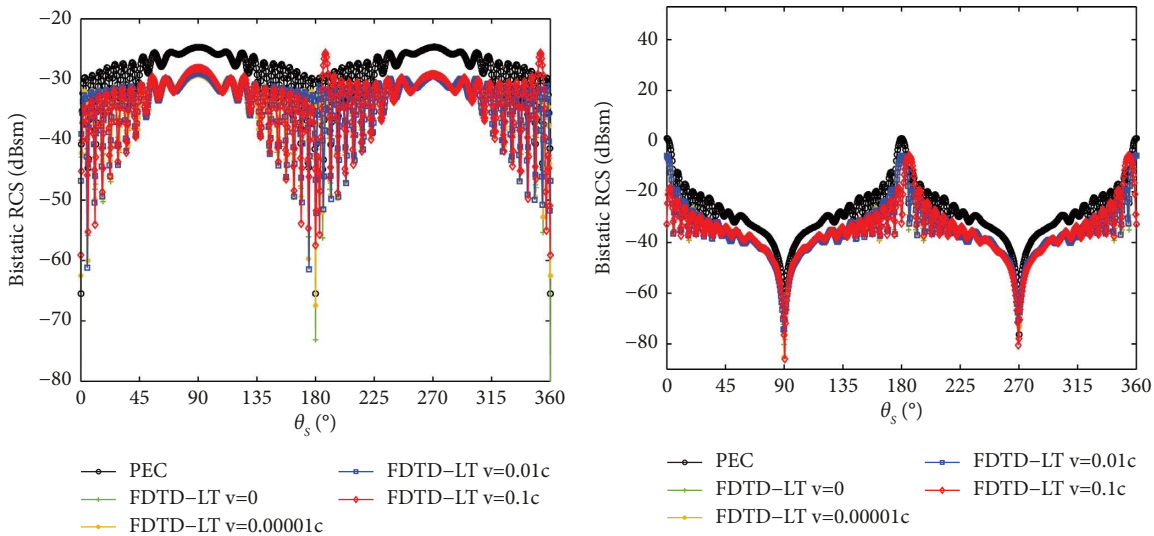

(a) (b)

Figure 5: Continued.

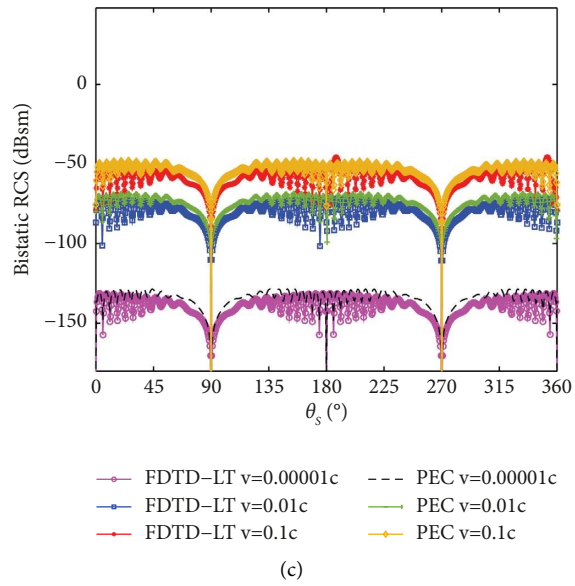

(c)

Figure 5: Polarized RCS for the plasma coated cylinder: (a) VH-polarization, (b) HH-polarization, and (c) RH-polarization.

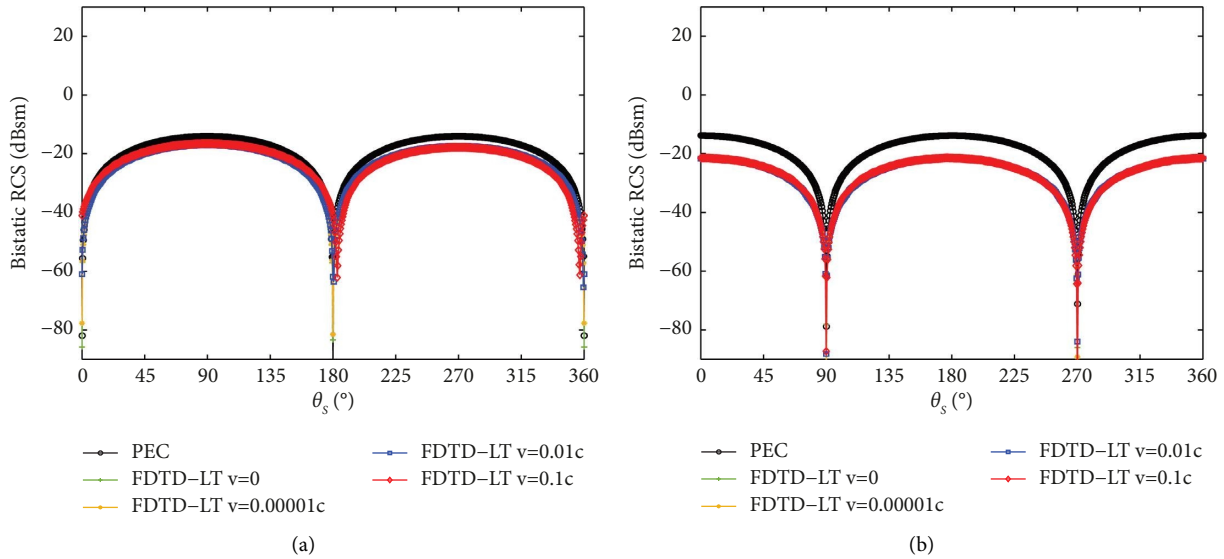

(a) (b)

Figure 6: Continued.

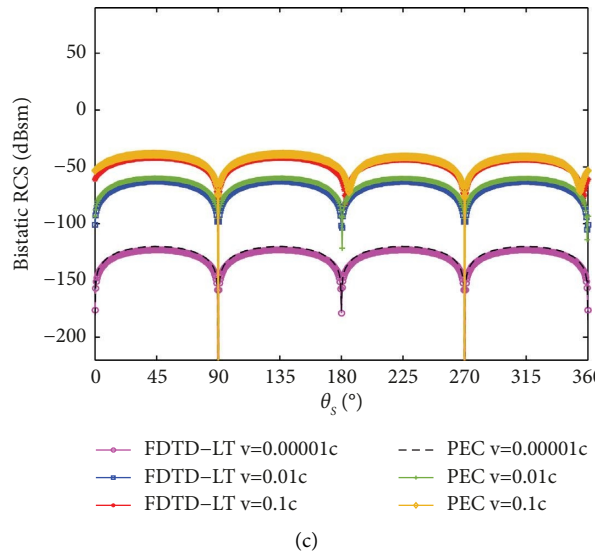

(c)

Figure 6: Polarized RCS for the plasma coated sphere: (a) VH-polarization, (b) HH-polarization, and (c) RH-polarization.

solution, as depicted in Figures 4(a) and 4(b). The simulation results obtained using the Lorentz-ADE-FDTD algorithm show excellent agreement with the analytical results, providing evidence of the accuracy of the Lorentz-ADE-FDTD algorithm. The motion of the object results in field component E_{sr}. Figure 4(c) depicts patterns of the RH-polarized RCS, arising from movements of the plasma cylinder. The increase in velocity is accompanied by an increase in the RH-polarized RCS component of the plasma cylinder, as shown in Figure 4(c). The patterns corresponding to different velocities of the RH-polarized RCS component exhibit noticeable differences, even at velocities below $0.01c$. In other words, the RH-polarized bistatic RCS component exhibits greater sensitivity to variations in velocity, in comparison with the VH-polarized bistatic RCS component and the HH-polarized bistatic RCS component.

Furthermore, a moving plasma coated cylinder object is considered. The PEC cylinder under the plasma layer has a radius of 0.09 m and a height of 0.38 m. The thickness of coated layer is 0.01 m. The material of the coated remains the same as used in the previous simulation. The angle of the incident wave is $(\theta_i = 90^\circ, \varphi_i = 90^\circ)$, and the motion direction of the object is perpendicular to the incident wave propagation direction. The frequency of the incident plane wave is 8GHz. The scattering angle φ_s is 0°. Figures 5(a)–5(c) presents the bistatic RCS as a function of θ_s for the object with various velocities, respectively. As the velocity of the plasma coated object increases, slight increases and decreases can be observed in the VH-polarized RCS component near the forward and backward scattering direction, respectively. In Figure 5(b), it is evident that the copolarized RCS has shifted significantly to the right near the scattering angle $\theta_s = 180^\circ$ and to the left near the scattering angle $\theta_s = 360^\circ$. Meanwhile, as shown in Figures 5(a) and 5(b), the bistatic scattering results of coated cylinder are lower than the results of PEC (perfectly electric conductor) cylinder. The patterns of the RH-polarized RCS resulting from the movement of the sphere are depicted in Figure 5(c). At the same speed, the RH-polarized RCS of the cylinder coated with plasma layer is around 5 dBsm lower than that of cylinder without the plasma coating layer. It is evident that the RH-polarized RCSs from the plasma coated cylinder are significantly decreased for different velocities.

Furthermore, a case of a plasma coated sphere in motion with the radius $r = 0.11$ m is proposed. The plasma coating layer has a thickness of 0.01 m. The material of the coated remains the same as used in the previous simulation. The angle of the incident wave is $(\theta_i = 90^\circ, \varphi_i = 90^\circ)$, and the motion direction of the object is perpendicular to the incident wave propagation direction. The frequency of the incident plane wave is 8GHz. The scattering angle φ_s is 0°. The comparison of the polarized (VH, HH, RH) bistatic scatterings from a plasma coated sphere with different velocities is shown in Figures 6(a)–6(c), respectively. As shown in Figure 6(a), in the range of scattering angle from 0° to 180°, VH-polarized bistatic RCS increases with increasing velocity. Within the scattering angle ranging from $\theta_s = 180^\circ$ to $\theta_s = 360^\circ$, the result of VH-polarized bistatic RCS decreases with increasing velocity. The bistatic HH-polarized RCSs show negligible variation with the change in the object's velocity. Meanwhile, as shown in Figures 6(a) and 6(b), the RCS of coated sphere is lower than the RCS of the PEC sphere. As depicted in Figure 6(c), the RH-polarized bistatic RCS increases with increasing velocity. The RH-polarized bistatic scattering results of coated sphere are lower than that of the PEC sphere. We can draw the conclusion that the plasma coating is still effective in decreasing the RH-polarized scatterings.

5. Conclusion

This manuscript presents a novel approach for computing the polarized scattering characteristics of a 3-D object with the plasma coated layer initially by utilizing the Lorentz-

ADE-FDTD algorithm. The relativistic electromagnetic polarized scattering characteristics from the object with plasma coating layered in motion are comparable to those of the stationary object since the velocity becomes lower than $0.01c$. When the velocity increases to $0.1c$, a distinct difference is observed in the RCS curve of the plasma coated object in motion compared to the stationary case. The motion of the object results in radial RCSs in the spherical coordinate system, which is absent in the case of a stationary object. The obtained results demonstrate a significant decrease in the bistatic polarized scatterings from the object coated with plasma for all velocities. This indicates that the plasma coating layer remains effective in decreasing the RCS, even when the object is in motion. The radial RCS can be utilized for the identification of high-speed moving objects. In further studies, we plan to extend the proposed method to investigate polarized scatterings from hypersonic reentry objects.

Data Availability

The data supporting the current study are available from the corresponding author upon request.

Conflicts of Interest

The authors declare that there are no conflicts of interest.

Acknowledgments

This work was supported in part by the National Natural Science Foundation of China under Grant 62271205, Grant 61871184, and Grant 61571190 and Science and Technology Commission of Shanghai Municipality 22DZ2229004.

References

[1] A. Taflove, *Computational Electrodynamics: The Finite-Difference Time-Domain Method*, Artech House, Norwood, MA, USA, 1995.

[2] R. J. Luebbers, F. Hunsberger, K. S. Kunz, R. B. Standler, and M. Schneider, "A frequency-dependent finite-difference time-domain formulation for dispersive materials," *IEEE Transactions on Electromagnetic Compatibility*, vol. 32, no. 3, pp. 222–227, 1990.

[3] R. J. Luebbers, F. Hunsberger, and K. S. Kunz, "A frequency-dependent finite-difference time-domain formulation for transient propagation in plasma," *IEEE Transactions on Antennas and Propagation*, vol. 39, no. 1, pp. 29–34, 1991.

[4] D. F. Kelley and R. Luebbers, "The piecewise linear recursive convolution method for incorporating dispersive media into FDTD," in *Proceedings of the 11th Rev in ACES*, pp. 526–533, Monterey, CA, USA, 1995.

[5] R. Siushansian and J. LoVetri, "An effective higher order numerical convolution for modeling Nth-order Lorentz dispersion," in *Proceedings of the IEEE Antennas and Propagation Symp*, pp. 632–635, Newport Beach, CA, USA, June 1995.

[6] A. Grande, I. Barba, A. Cabeceira, J. Represa, P. So, and W. Hoefer, "FDTD modeling of transient microwave signals in dispersive and lossy bi-isotropic media," *IEEE Transactions on Microwave Theory and Techniques*, vol. 52, no. 3, pp. 773–784, 2004.

[7] A. Akyurtlu and D. H. Werner, "A novel dispersive FDTD formulation for modeling transient propagation in chiral metamaterials," *IEEE Transactions on Antennas and Propagation*, vol. 52, no. 9, pp. 2267–2276, 2004.

[8] J. Y. Lee, J. H. Lee, H. S. Kim, N. W. Kang, and H. K. Jung, "Effective medium approach of left-handed material using a dispersive FDTD method," *IEEE Transactions on Magnetics*, vol. 41, no. 5, pp. 1484–1487, 2005.

[9] D. M. Sullivan, "Frequency-dependent FDTD methods using Z-transforms," *IEEE Transactions on Antennas and Propagation*, vol. 40, no. 10, pp. 1223–1230, 1992.

[10] T. Kashiwa, N. Yoshida, and I. Fukai, "A treatment by the finite-difference time-domain method of the dispersive characteristic associated with orientation polarization," *Inst Electron Inform Communicat Eng (Japan) Trans*, vol. 37, no. 8, pp. 1326–1328, 1990.

[11] R. M. Joseph, S. C. Hagness, and A. Taflove, "Direct time integration of Maxwell's equations in linear dispersive media with absorption for scattering and propagation of femto second electromagnetic pulses," *Optics Letters*, vol. 16, no. 18, pp. 1412–1414, 1991.

[12] O. Gandhi, B. Q. Gao, and J. Y. Chen, "A frequency-dependent finite-difference time domain formulation for general dispersive media," *IEEE Transactions on Microwave Theory and Techniques*, vol. 41, no. 4, pp. 658–665, 1993.

[13] T. Kashiwa, Y. Ohtomo, and I. Fukai, "Formulation of dispersive characteristics associated with orientation polarization using the FDTD method," *Electronics and Communications in Japan*, vol. 75, no. 6, pp. 87–96, 1992.

[14] T. Kashiwa and I. Fukai, "A treatment by the FD-TD method of the dispersive characteristics associated with electronic polarization," *Microwave and Optical Technology Letters*, vol. 3, no. 6, pp. 203–205, 1990.

[15] P. M. Goorjian and A. Taflove, "Direct time integration of Maxwell's equations in nonlinear dispersive media for propagation and scattering of femtosecond electromagnetic solitons," *Optics Letters*, vol. 17, no. 3, pp. 180–182, 1992.

[16] O. P. Gandhi, B. Q. Gao, and J. Y. Chen, "A frequency-dependent finite-difference time-domain formulation for induced current calculations in human beings," *Bioelectromagnetics*, vol. 13, no. 6, pp. 543–555, 1992.

[17] L. Lu, C. Parini, and Y. Hao, "Dispersive FDTD characterisation of no phase-delay radio transmission over layered left-handed meta-materials structure," *IEE Proceedings-Science, Measurement and Technology*, vol. 151, no. 6, pp. 403–406, 2004.

[18] J. Van Bladel, *Relativity and Engineering*, Springer-Verlag, Berlin, Germany, 1984.

[19] F. Harfoush, A. Taflove, and G. A. Kriegsmann, "A numerical technique for analyzing electromagnetic wave scattering from moving surfaces in one and two dimensions," *IEEE Transactions on Antennas and Propagation*, vol. 37, no. 1, pp. 55–63, 1989.

[20] F. Harfoush, A. Taflove, and G. A. Kriegsmann, "Numerical implementation of relativistic electromagnetic boundary conditions in a laboratory-frame grid," *Journal of Computational Physics*, vol. 89, no. 1, pp. 80–94, 1990.

[21] L. Kuang, S. Zhu, J. Gao, Z. Zheng, and D. Dong, "A numerical method for analyzing electromagnetic scattering properties of a moving conducting object," *International Journal of Antennas and Propagation*, vol. 2014, Article ID 386315, 9 pages, 2014.

[22] K. S. Zheng, J. Li, G. Wei, and J. Xu, "Analysis of Doppler effect of moving conducting surfaces with Lorentz-FDTD method," *Journal of Electromagnetic Waves and Applications*, vol. 27, no. 2, pp. 149–159, 2013.

[23] K. S. Zheng, Z. M. Mu, H. Luo, and G. Wei, "Electromagnetic properties from moving dielectric in high speed with Lorentz-FDTD," *IEEE Antennas and Wireless Propagation Letters*, vol. 15, pp. 934–937, 2016.

[24] L. Kuang, F. Xu, S. Z. Zhu, J. J. Gao, and Z. Q. Zheng, "Relativistic FDTD analysis of far-field scattering of a high-speed moving object," *IEEE Antennas and Wireless Propagation Letters*, vol. 14, pp. 879–882, 2015.

[25] K. S. Zheng, Y. J. Li, L. F. Xu, J. Z. Li, and G. Wei, "Electromagnetic properties of a complex pyramid-shaped target moving at high speed," *IEEE Transactions on Antennas and Propagation*, vol. 66, no. 12, pp. 7472–7476, 2018.

[26] Y. Zhao and S. Chaimool, "Relativistic finite-difference time domain analysis of high-speed moving metamaterials," *Scientific Reports*, vol. 8, no. 1, p. 7686, 2018.

[27] A. A. Tzikas, D. P. Chrissoulidis, and E. E. Kriezis, "Relativistic bistatic scattering by a uniformly moving random rough surface," *IEEE Transactions on Antennas and Propagation*, vol. 34, no. 8, pp. 1046–1052, 1986.

[28] P. Ren, L. Kuang, J. Gao, and Q. Liu, "FDTD analysis of relativistic bistatic polarized scattering from a high-speed moving dielectric coated target," *IEEE Access*, vol. 11, pp. 34486–34497, 2023.

[29] C. Yeh, "Reflection and transmission of electromagnetic waves by a moving plasma medium. II. Parallel polarizations," *Journal of Applied Physics*, vol. 38, no. 7, pp. 2871–2873, 1967.